

Effects of refraction on transmission spectra of gas giants: decrease of the Rayleigh scattering slope and breaking of retrieval degeneracies

Yan Bétrémieux¹ *

¹*Max-Planck-Institut für Astronomie, Königstuhl 17, D-69117 Heidelberg, Germany*

13 June 2021

ABSTRACT

Detection of the signature of Rayleigh scattering in the transmission spectrum of an exoplanet is increasingly becoming the target of observational campaigns because the spectral slope of the Rayleigh continuum enables one to determine the scaleheight of its atmosphere in the absence of hazes. However, this is only true when one ignores the refractive effects of the exoplanet’s atmosphere. I illustrate with a suite of simple isothermal clear Jovian H₂-He atmosphere models with various abundances of water that refraction can decrease significantly the spectral slope of the Rayleigh continuum and that it becomes flat in the infrared. This mimics a surface, or an optically thick cloud deck, at much smaller pressures than one can probe in the non-refractive case. The relative impact of refraction on an exoplanet’s transmission spectrum decreases with atmospheric temperatures and increases with stellar temperature. Refraction is quite important from a retrieval’s perspective for Jovian-like planets even at the highest atmospheric temperatures (1200 K) considered in this paper, and for all stellar spectral types. Indeed, refraction breaks in large part the retrieval degeneracy between abundances of chemical species and the planet’s radius because the size of spectral features increases significantly with abundances, in stark contrast with the non-refractive case which simply shifts them to a larger or smaller effective radius. Abundances inferred assuming the atmosphere is cloud-free are lower limits. These results show how important it is to include refraction in retrieval algorithms to interpret transmission spectra of gas giants accurately.

Key words: atmospheric effects – methods: numerical – planets and satellites: atmospheres – planets and satellites: gaseous planets – radiative transfer.

1 INTRODUCTION

Transmission spectroscopy is a powerful observational method that allows one to probe the atmosphere of a transiting exoplanet. Occultation by the body of the planet and absorption by the planetary atmosphere cause a drop in the stellar flux during the planetary transit. The absorption cross section of the exoplanet as a function of wavelength, expressed in terms of its effective radius (Brown 2001), depends on the transmission of the atmosphere at the terminator as a function of altitude, as well as the radius of the planet at a reference atmospheric pressure.

To understand which atmospheric parameters can be retrieved from the analysis of transmission spectra, Lecavelier des Etangs et al. (2008) derived a few simple

relationships for an isothermal atmosphere with a uniform vertical composition. They showed numerically that the effective radius of an exoplanet occurs at an altitude where the integrated optical depth along the line of sight grazing the planetary limb, or slant optical depth, is about 0.56. This was later demonstrated analytically by de Wit & Seager (2013). Using this simple relation, Lecavelier des Etangs et al. (2008) also showed that the size of spectral features scales with the atmospheric scaleheight. Assuming H₂ Rayleigh scattering to be the most important source of extinction from 0.6 to 1 μm , they derived the scaleheight, and hence the temperature, of HD 189733b from transit data obtained with the Hubble Space Telescope (Pont et al. 2008).

Since the spectral dependence of Rayleigh scattering cross sections is well known, spectral regions dominated by Rayleigh scattering are particularly useful to deter-

* personal e-mail: yanbet@yahoo.com

mine the scaleheight of an atmosphere by measuring the change in the effective planetary radius with wavelength (Lecavelier des Etangs et al. 2008; Benneke & Seager 2012; Howe & Burrows 2012). This Rayleigh slope can be used to discriminate between various bulk atmospheric composition, provided the atmosphere is relatively clear of hazes or clouds. In the presence of extended vertical hazes, the transmission spectrum will instead bear the signature of the hazes' optical properties (Howe & Burrows 2012; Robinson et al. 2014; Wakeford & Sing 2015). Either way, this slope provides an important constraint on the properties of exoplanetary atmospheres, and has been detected in a few exoplanets, e.g. HD 209458b (Knutson et al. 2007; Sing et al. 2008), HD 189733b (Pont et al. 2008), HAT-P-5b (Southworth et al. 2012), WASP-12b (Sing et al. 2013), GJ 3470b (Nascimbeni et al. 2013), WASP-6b (Jordán et al. 2013; Nikolov et al. 2015), Qatar-2b (Mancini et al. 2014), WASP-31b (Sing et al. 2015), and WASP-103b (Southworth et al. 2015).

In spectral region where molecular absorption dominates, the atmospheric scaleheight can still be estimated from the size of absorption features if one assumes that molecules are well-mixed in the atmosphere. However, it is very difficult to determine the absolute abundances of species and the pressure regions that are probed, as degenerate solutions exist which can match observations. Indeed, changes of several orders of magnitude in molecular abundances can be compensated with a small change in the planetary radius at the reference pressure (Griffith 2014). Although the absolute mole fraction of species is ambiguous, their relative abundances are well constrained through the relative strength of absorption features (Benneke & Seager 2012) in a haze-free atmosphere.

However, none of these previous investigations of the retrieval of atmospheric parameters considers the refractive effects of the exoplanetary atmosphere on its transmission spectrum, in stark contrast with stellar occultations. The use of refractive effects to probe planetary atmospheres has a long standing history in Solar system exploration which started with the occultation of σ Arietis by the atmosphere of Jupiter (Baum & Code 1953). This pioneering work paved the way for stellar occultation by planetary atmospheres to become a powerful method by which one can derive not only the density vertical profile of planetary atmospheres, but also deduce the vertical profile of minor chemical species which absorb stellar radiation (see the review by Smith & Hunten 1990). However, the observational geometry of a stellar occultation is different from that of a transiting exoplanet. Indeed, in a stellar occultation, the radiation source is infinitely far away compared to the planet and the observer, whereas in an exoplanet transit geometry the observer is infinitely far away from the exoplanet and its star.

Hubbard et al. (2001) first investigated the impact of refraction on exoplanet transmission spectra and deduced that refractive effects were negligible for the hot Jupiter HD 209458b. However, Hui & Seager (2002) adapted gravitational microlensing theory to atmospheric refraction and showed that refraction could be important for some transiting exoplanets. Sidis & Sari (2010) used a more conventional ray-tracing approach and came to the same conclusion. They both found that even in

the absence of absorption, an exoplanet's effective radius is still quite large because the higher density regions of planetary atmospheres deflect stellar radiation away from the observer. Absorption by chemical species were later combined with ray-tracing (García Muñoz et al. 2012; Bétrémieux & Kaltenegger 2013; Misra, Meadows & Crisp 2014) to compute transmission spectra of an Earth-Sun analog, and showed that refraction decreases significantly the contrast of H₂O features because transmission spectroscopy cannot probe most of the troposphere, which holds the bulk of Earth's water inventory.

Bétrémieux & Kaltenegger (2014) explored the parameter space of an Earth-like planet receiving the same stellar flux as Venus, Earth, and Mars, for different spectral type host stars along the Main Sequence. They showed that one can only probe an Earth-like planet with the same insolation as Earth to a pressure of 1 bar if the planet orbits a M5 or cooler star, assuming it maintains a similar temperature-pressure profile. As the temperature of the host star increases, the contrast of spectral features decreases, potentially resulting in flat spectral regions (see their Figure 11). Refraction also produces wings brighter than the continuum just outside of transit (Hui & Seager 2002; Sidis & Sari 2010; García Muñoz et al. 2012) because some of the stellar radiation is deflected toward the observer while the star is unocculted. These brighter wings are sensitive to the aerosol content of an atmosphere (Misra & Meadows 2014).

More recently, Bétrémieux & Kaltenegger (2015) developed new analytical expressions to describe the integrated column abundance along the curved path of a refracted ray, as well as the total deflection of the ray. They discovered that thick atmospheres form a thin refractive boundary layer where the column abundance and its deflection, go from finite to infinite values as the grazing altitude of a ray decreases and approaches a lower refractive boundary. Indeed, at this lower boundary, the radius of curvature of the ray induced by refraction matches the radial position at which the ray grazes the atmosphere, and the ray follows a closed circular path. These results diverge substantially from expressions developed for stellar occultations (Baum & Code 1953) and still in use today. Rays that penetrate below this lower boundary will spiral into the atmosphere and be absorbed. Hence, atmospheric regions located below this lower boundary cannot be probed by techniques based on the transmission of radiation through an atmosphere, irrespective of the planet-star geometry. Furthermore, the effective scaleheight of the atmosphere, i.e. as perceived by an observer, decreases dramatically as this lower boundary is approached.

What impact does refraction, and in particular this new theory, has on transmission spectroscopy of giant exoplanets? Does it affect the Rayleigh scattering slope, or the retrieval of atmospheric parameters? This paper explores these issues for Jupiter-sized planets with a Jovian composition across various planetary temperatures and spectral type of the host star.

2 DETAILS OF SIMULATIONS

To illustrate the impact of refraction on transmission spectroscopy of giant planets and on the retrieval of their atmospheric properties, I compute a suite of transmis-

sion spectra from 0.4 to 5.0 μm for a Jovian-like planet with a H_2 -He atmosphere orbiting stars of different spectral type along the Main Sequence (M2, K5, G2, F0). I consider isothermal spherically-symmetric well-mixed atmospheres for three different temperatures (300, 600, and 1200 K), and various constant mole fractions of water vapour (0, 10^{-12} , 10^{-10} , 10^{-8} , 10^{-6} , and 10^{-4}). These simulations are done both with and without refraction. Stellar limb-darkening is ignored in these simulations, just as it was ignored in all derivations of the Rayleigh slope (Lecavelier des Etangs et al. 2008; Benneke & Seager 2012; Howe & Burrows 2012; de Wit & Seager 2013), to have a common reference frame and enable a direct comparison with previous simulations of transit spectra. Much of the theory and methods at the heart of these simulations have already been described in detail (B  tr  mieux & Kaltenegger 2013, 2014, 2015), but are summarised in this section for the convenience of the readers.

2.1 Planetary atmospheres

I build-up the density vertical profile of an isothermal homogeneous atmospheres in hydrostatic equilibrium with a gravitational acceleration which varies with altitude, for three different temperatures (300, 600, and 1200 K), in the manner described in Section 3.3 in B  tr  mieux & Kaltenegger (2015). The radius ($R_P = 69911$ km) and mass ($M_P = 1.8986 \times 10^{27}$ kg) of the exoplanet are the same as Jupiter’s. The atmosphere has a He mole fraction of 0.1357, as measured on Jupiter by the Galileo probe (listed in Lodders & Fegley Jr. 1998), while the remainder of the atmosphere is predominantly composed of H_2 and trace amounts of water. The planetary radius (R_p) is defined at a reference pressure of 1 atm (atmosphere), and the highest pressure considered in the simulations, or “surface” pressure, is 500 atm. The densities are computed on a fine computational grid with thickness Δz_{comp} , and then sampled on a coarser grid with altitude intervals Δz_{samp} . Table 1 lists the thickness of the layers making the computational and sampling grids, along with the chosen atmospheric thickness (ΔZ_{atm}), and the resulting “surface” altitude (z_s) for each temperature. The atmospheric thickness defines the radius of the top atmospheric boundary (R_{top}), given by

$$R_{top} = R_p + z_s + \Delta Z_{atm}. \quad (1)$$

2.2 Planet-star distance

To determine the distance between the planet and its stellar host, I assume that the isothermal temperature of the planet (T_p) matches the mean planetary emission temperature and that the planet has a circular orbit. Under these assumptions, the semi-major axis (a) of the planet is given by,

$$a = \frac{\sqrt{1 - \Lambda_B}}{2} \left(\frac{T_*}{T_p} \right)^2 R_* \quad (2)$$

where Λ_B is the Bond albedo of the planet, while T_* and R_* are the stellar effective temperature and radius, respectively. Table 2 lists these stellar parameters for the four stellar spectral type (M2, K5, G2, F0) along the Main Sequence

Table 1. Input and derived model atmosphere parameters for different atmospheric temperatures

Input			
T_p (K)	300	600	1200
ΔZ_{atm} (km)	1370	2760	5640
Δz_{samp} (km)	5	10	20
Δz_{comp} (km)	0.01	0.02	0.04
Derived			
z_s (km)	-260.70	-519.48	-1031.28

Table 2. Stellar parameters (Cox 2000)

Spectral type	T_* (K)	R_* (R_\odot)
F0	7300	1.50
G2	5778 ^a	1.00
K5	4410	0.72
M2 ^b	3400	0.44

^a Lodders & Fegley Jr. (1998)

^b values from Reid & Hawley (2005)

considered in this paper. A Bond albedo of 0.30 is chosen, similar to those of the giant planets in our Solar system.

2.3 Column abundances and ray deflection

To compute the transmission spectrum of an exoplanet, one must determine the altitude-dependent incremental column abundance encountered by a ray along its curved refracted path, as well as the total deflection of the ray, as a function of a ray’s grazing height (r_0), i.e. planetary radius + grazing altitude of the ray. I compute these quantities with MAKEX-OSHELL (see Section 3 in B  tr  mieux & Kaltenegger 2015), including the contribution from atmospheric regions above the top atmospheric boundary, with 80 rays spread uniformly in grazing altitude between the top and bottom boundaries. These grazing altitudes also define the boundaries of the atmospheric layers used in the computation. For the refractive case, I use a refractivity at standard temperature and pressure (ν_{STP}) of 1.23×10^{-4} , that of the Jovian atmosphere at 1 μm , and a refractivity of 0 otherwise. The location of the bottom atmospheric boundary depends on the condition of the simulations. In the refractive case, the bottom boundary can be either the critical or the lower refractive boundary (see Section 2.4), otherwise the bottom boundary is the “surface”.

2.4 Critical and lower refractive boundaries

The lower refractive boundary is located at a height (r) where, in a spherically symmetric atmosphere, a grazing ray follows a circular path (see Section 2.2 in B  tr  mieux & Kaltenegger 2015). Atmospheric regions below this boundary cannot be probed by exoplanet transmission spectroscopy or by stellar occultations because rays

Table 3. Refractive boundaries of Jupiter-sized planets with different isothermal temperatures orbiting stars of various spectral type (see Section 2.4)

T (K)	300		600		1200	
Critical Boundary	n (amagat ^a)	P (bar)	n (amagat)	P (bar)	n (amagat)	P (bar)
F0 star	0.33	0.37	1.78	3.97	8.64	38.45
G2 star	0.54	0.60	2.78	6.20	12.21	54.34
K5 star	0.92	1.02	4.45	9.90	16.25	72.35
M2 star	1.56	1.73	6.62	14.74	18.75	83.45
Lower Boundary ^b	4.88	5.43	9.74	21.69	19.38	86.27

^a 1 amagat = density at standard temperature and pressure (STP)

^b independent of stellar spectral type

that reach these regions spiral deeper into the atmosphere until they are absorbed. This boundary is located at a height where

$$\left(\frac{\nu(r)}{1 + \nu(r)}\right) \frac{r}{H} = 1, \quad (3)$$

and this depends only on the properties of the atmosphere. Here, $\nu(r)$ is the height-dependent refractivity of the atmosphere, and H is the density scale height.

In reality, one can only probe to the critical refractive boundary (see Section 2.2 in Bétrémieux & Kaltenegger 2014). This boundary occurs at a density where the atmosphere deflects a ray coming from the opposite stellar limb toward the observer. Hence, this boundary depends both on the properties of the atmosphere and on the geometry of the planet-star system, i.e. on the angular size of the star as seen from the planet. When the planet occults the central region of its host star, this boundary is located at the same density all around the planetary limb, where rays are deflected by a critical deflection (ω_c). During the course of a transit, this symmetry is broken and one can probe higher densities on one side of the planet, and lower densities on the opposite side. However, since the ray deflection tends to infinity as the grazing height of the ray approaches the lower boundary, the critical boundary can only asymptotically approach but never reach the lower boundary.

MAKEXOSHELL computes the quantity on the left-hand side of equation 3 on the fine altitude computational grid, and determines the lower boundary by choosing the altitude for which this value is closest to but less than one. I also use MAKEXOSHELL to find the location of the critical boundary by computing the ray deflection for a grid of grazing heights, and then determine which one has the smallest difference with the critical deflection of the planet-star system, which is given by

$$\sin \omega_c = \frac{r_0 + R_*}{a}. \quad (4)$$

Table 3 shows the critical boundaries for the four spectral type stars from Table 2, both in terms of the density and pressure of the atmosphere, for the three isothermal temperatures considered. It also lists the lower boundaries which are independent of the spectral type of the host star.

2.5 Radiative transfer

The radiative transfer code (Bétrémieux & Kaltenegger 2013) combines the MAKEXOSHELL-computed column abundances (N_{ik}) of the k^{th} atmospheric layer encountered by the i^{th} ray, with the average mole fraction (f_{ijk}) and extinction cross section (σ_j) of the j^{th} chemical species, to compute the integrated optical depth (τ_i) along the i^{th} ray, using

$$\tau_i = \sum_k \bar{\sigma}_{ik} N_{ik}, \quad (5)$$

where

$$\bar{\sigma}_{ik} = \sum_j \sigma_j f_{ijk} \quad (6)$$

is the average extinction cross section of the k^{th} layer along the i^{th} ray. Since all the molecular species are well-mixed in these simulations, f_{ijk} is independent of the atmospheric layer and of the ray, and is simply the average mole fraction of the j^{th} species. The transmission (T_i) of the i^{th} ray is simply given by

$$T_i = e^{-\tau_i}. \quad (7)$$

Earlier versions of the code (see e.g. Johnson et al. 1995; Kaltenegger & Traub 2009) added thermal emission to the transmitted stellar radiation. However, for a one-dimensional spherically symmetric atmosphere, the thermal emission contribution to an exoplanet light curve is constant throughout the transit, and the calculated transit depth is independent of thermal emission. To save on computation time, Bétrémieux & Kaltenegger (2013) modified the code so that one can choose not to include thermal emission.

Although the line opacity database is identical to that in Kaltenegger & Traub (2009), Bétrémieux & Kaltenegger (2013) replaced the original Rayleigh scattering parametrisation, appropriate only for Earth, with a database of Rayleigh scattering cross sections for N₂, O₂, CO₂, and Ar (see their Table 2). They also included new routines to compute optical depths from continuous absorption cross sections, and a new database of ultraviolet and visible absorbers (see their Table 1).

For this paper, I have added the Rayleigh scattering cross section of molecular hydrogen and helium to the database. I use the formulation by Ford & Browne (1973)

for the H₂ cross section as a function of its rotational quantum number J , from which I compute the cross section for an equilibrium H₂ population at 300 K. Since the temperature dependence of the cross section is very small (e.g. about 0.6 per cent change between 273.15 and 2000 K at 1 μm), I use the 300 K cross section for all temperatures. For helium, I compute its STP refractivity with the expression from Mansfield & Peck (1969), also described in Weber (2003), and obtain its Rayleigh cross section (σ_R) with Rayleigh’s formula:

$$\sigma_R = \frac{32\pi^3}{3} \left(\frac{\nu_{STP}}{n_{STP}} \right)^2 w^4 F_K. \quad (8)$$

Here, n_{STP} is the number density at standard temperature and pressure, also known as Loschmidt’s number, w is the wavenumber of the radiation, and F_K is the King correction factor. For helium, F_K is equal to one at all wavenumbers.

The only other source of opacity considered in these simulations is that of water vapour. The algorithm for the line-by-line computation of optical depths is described in Traub & Stier (1976). To reduce the computation time, only H₂O lines which have a peak optical depth greater than 10^{-7} within an atmospheric layer are included, and the line profile is computed to an optical depth of 10^{-8} or to the edge of the spectral region, whichever is closer to the centre of the line. The atmospheric transmission is computed from 1800 to 26000 cm^{-1} every 0.05 cm^{-1} , and then averaged in 4 cm^{-1} -wide bins. I choose a spectral region which is larger than that of interest to mitigate edge effects. The transmission spectrum is eventually displayed with respect to wavelength from 0.4 to 5.0 μm .

To compute the effective radius (R_{eff}) of the transiting exoplanet, I use the 80 rays from MAKEXOSHELL (see Section 2.3) to partition the atmosphere into 80 annuli evenly spread in altitude. I then map these altitude boundaries to their corresponding impact parameter (b_i) across the planetary limb, which is what an observer perceives. The impact parameter is given by

$$b_i = (1 + \nu(r_{0i}))r_{0i}. \quad (9)$$

Taking the transmission of each annulus to be the average of the transmission at the boundaries, and ignoring stellar limb-darkening, the effective radius is then given by

$$R_{eff}^2 = R_{top}^2 - \sum_{i=1}^N \left(\frac{T_{i+1} + T_i}{2} \right) (b_{i+1}^2 - b_i^2) \quad (10)$$

(B  tr  mieux & Kaltenecker 2013) where N is the number of annuli. The $(N + 1)^{th}$ ray is that which grazes the top atmospheric boundary, chosen so that both atmospheric absorption and deflection are negligible. Thus $T_{N+1} = 1$, and $b_{N+1} = R_{top}$. Atmospheric regions with densities higher than the density at the lower atmospheric boundary (i.e. the “surface”, lower refractive boundary, or critical refractive boundary depending on the simulation) are implicitly assumed to be opaque at all wavelengths. One advantage to including refraction is that one does not need to compute the transmission of atmospheric regions located at higher densities and pressures, or lower altitude, than the lower refractive boundary. I display the transmission spectrum in terms of the effective atmospheric thickness (Δz_{eff}) of the transiting exoplanet with respect to the 500 atm “surface”,

which I compute with

$$\Delta z_{eff} = R_{eff} - (R_p + z_s). \quad (11)$$

3 RESULTS AND DISCUSSION

3.1 Rayleigh scattering slope

To explore how refraction affects the Rayleigh scattering slope, I first compute transmission spectra where the only source of opacity is Rayleigh scattering from H₂ and He. Figures 1 through 3 show the 0.4-5.0 μm H₂-He Rayleigh continuum under various conditions for the 300, 600, and 1200 K isothermal atmospheres, respectively. The legends in all three figures are identical. The 500 atm “surface” is located at 0 km altitude, and the 1 atm pressure level is indicated for reference. Since the main effect of temperature is to change the scale height of the atmosphere, I scale the range of values on the ordinate with the planetary temperature so that approximately the same number of scaleheight are displayed in all figures. It is not exactly the same because the gravitational acceleration varies with altitude in the simulations, and so does the scaleheight. It is useful to plot things this way to notice secondary effects subtler than the primary effect of the scaling of spectral features with scaleheight. Indeed, even if transmission spectra have the same aspect from one figure to the next, the actual size of spectral features still differ by roughly the ratio of the planetary temperatures. I have done this in all figures throughout the paper.

Without refraction, the transmission spectrum of a Rayleigh scattering isothermal atmosphere should follow a straight line when plotted in terms of the effective atmospheric thickness versus the natural logarithm of the wavelength (Lecavelier des Etangs et al. 2008; Benneke & Seager 2012; Howe & Burrows 2012), as long as the Rayleigh scattering cross section follows a constant power law with wavelength. The Rayleigh continuum for the non-refractive case (shown by the short-dashed line in all three figures) has roughly a constant slope except longward of 3 μm where the Rayleigh cross section is sufficiently weak that the opaque regions below the “surface” contribute significantly to the transmission spectrum. In this case, these regions introduce a significant step function in the altitude-dependent atmospheric transmission profile, thus violating the conditions under which the result from Lecavelier des Etangs et al. (2008) holds, and changing the Rayleigh slope.

A noticeable secondary effect is that the spectrum also shifts to lower altitudes with increasing temperatures. This occurs because I reference the planetary radius to a pressure, as is often done (e.g. Benneke & Seager 2012; Swain, Line, & Deroo 2014), rather than to a density. As temperature increases, the same pressure is achieved with lower densities. Thus the densities required to achieve a slant optical thickness of 0.56 are located at lower altitudes and the transmission spectrum has an extra downward shift, beyond the primary scaleheight-induced factor, as the planetary temperature increases. It would seem that referencing the planetary radius to a density would be a better choice as the transmission spectrum would not shift up or down with temperature,

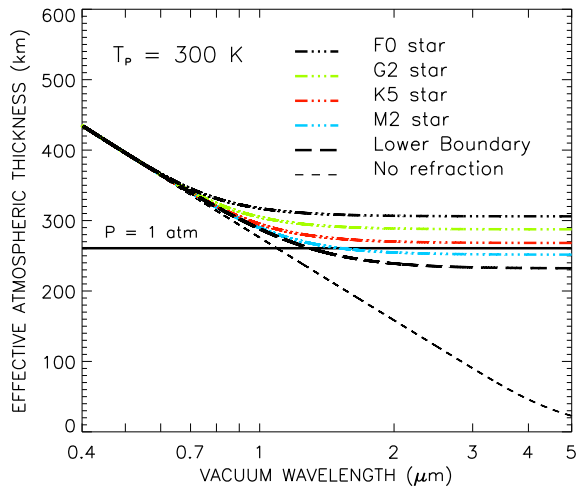


Figure 1. H₂-He Rayleigh scattering transmission spectra of a Jupiter-sized exoplanet with a 300 K isothermal Jovian atmosphere, expressed in term of the atmosphere’s effective thickness above the 500 atm pressure level (as for all figures). The short-dashed line shows the spectrum without refraction, while the coloured triple-dot-dashed lines show spectra with refraction for different Main Sequence spectral type of the host star. The long-dashed line shows the spectrum with refraction if one could somehow probe the atmosphere to the lower refractive boundary, irrespective of the planet-star distance. The thick horizontal solid line shows the altitude of the 1 atm pressure level, for reference (shown in all figures). See Table 3 for the density and pressure levels of the critical and lower refractive boundaries.

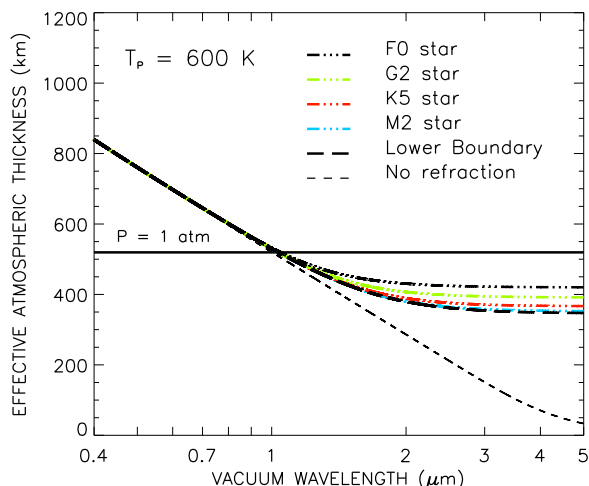


Figure 2. H₂-He Rayleigh scattering transmission spectra of a Jupiter-sized exoplanet with a 600 K isothermal Jovian atmosphere. See caption in Fig. 1 for more details.

but I nevertheless adopt this common convention in this paper.

In the refractive case, this simple picture changes dramatically. Indeed, the black long-dashed line shows the transmission spectrum if one can somehow probe to the lower refractive boundary, irrespective of the planet-star dis-

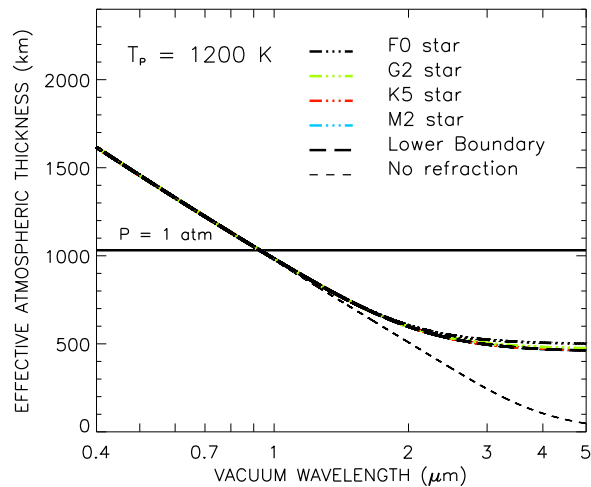


Figure 3. H₂-He Rayleigh scattering transmission spectra of a Jupiter-sized exoplanet with a 1200 K isothermal Jovian atmosphere. See caption in Fig. 1 for more details.

tance, which produces the smallest differences between the refractive and non-refractive cases. The infrared transmission spectrum is flat, similar to that of an optically thick cloud or a surface, and gradually merges with the non-refractive case at lower wavelengths. The wavelength above which the Rayleigh slope deviates significantly from the non-refractive case increases with temperature, and changes from about 0.6 μm at 300 K to about 1 μm at 1200 K. The fractional change of the spectrum with and without refraction increases with wavelength and decreases with temperature, and it is still quite important even at 1200 K above 3 μm .

Accounting for the location of the critical boundary associated with the spectral type of the host star increases the effective thickness of the atmosphere and changes the Rayleigh slope further (see triple-dotted dashed coloured lines in Figures 1 through 3). This correction can be quite important at the cooler planetary temperatures (see Figure 1). As the temperature of the planet increases, the differences between the spectra associated with a F0 and a M2 star decrease. At 1200 K (see Figure 3), there is hardly any differences between the transmission spectrum around a F0 and a M2 star, and both are very similar to the spectrum where one can probe to the lower refractive boundary. Indeed, as the planetary temperature increases, the critical boundary approaches the lower refractive boundary. Since the effective atmospheric scaleheight decreases dramatically at the approach of the lower refractive boundary (see Section 4.2.3 in Bétrémieux & Kaltenecker 2015), the altitude separation between the different critical boundaries also decreases.

Hence, the discovery of the refractive boundary layer by Bétrémieux & Kaltenecker (2015) turns out to be extremely important for the transmission spectra of giant exoplanets, because even in the absence of clouds or hazes, one cannot probe the atmosphere to arbitrarily large pressures in spectral regions between molecular bands. Indeed, this refractive boundary layer not only mimics a surface but also decreases substantially the effective scaleheight of the atmosphere near that boundary. This, in turns, modifies not only the effec-

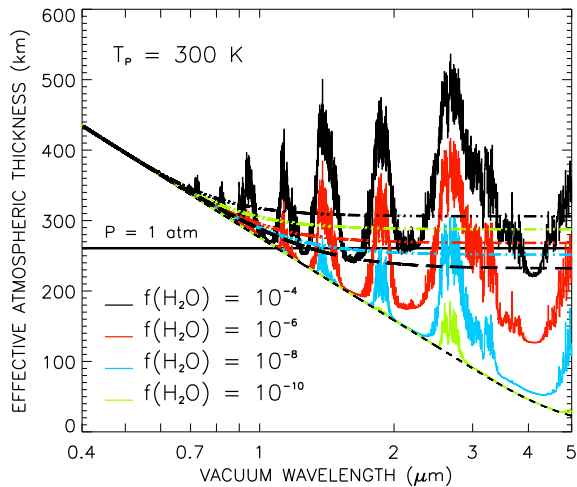


Figure 4. Transmission spectra without refraction of a Jupiter-sized exoplanet with a 300 K isothermal Jovian atmosphere for various vertical homogeneous mole fractions of water (see inset legend). The water-free Rayleigh scattering transmission spectra from Fig. 1 are overlaid for comparison (see caption and inset legend in Fig. 1 for more details). Refraction will suppress water features which lie below the refractive Rayleigh curve associated with the host star’s spectral type (coloured triple-dotted dashed lines).

tive radius of the Rayleigh continuum of the hotter exoplanets, but also decreases the Rayleigh scattering slope of the transmission spectrum. If one wants to infer the atmospheric scaleheight (Lecavelier des Etangs et al. 2008) or the mass of the exoplanet (de Wit & Seager 2013) from transmission spectra, one must be careful to evaluate the Rayleigh scattering slope in spectral regions that are largely unaffected by refraction, given the planetary temperatures. However, even then, the Rayleigh slope might still be affected by clouds or hazes, depending on their vertical distribution.

3.2 Abundance retrieval

To explore how refraction affects the retrieval of atmospheric abundances of chemical species, I now add various mole fractions of vertically-mixed water vapour (10^{-12} , 10^{-10} , 10^{-8} , 10^{-6} , and 10^{-4}) to the simulations. I use water vapour as an example because its spectral signature is often sought after in exoplanetary transmission spectra, but the discussion in this section is generally applicable to other molecules (e.g. CH_4 , NH_3 , CO , CO_2) as well.

Figure 4 shows the resulting transmission spectra (coloured solid lines) in the non-refractive case for the 300 K isothermal atmosphere compared with the various Rayleigh continua from Figure 1. Note that a H_2O mole fraction of 10^{-12} does not produce any noticeable absorption features above the Rayleigh continuum and is not shown. Changing the water abundance mostly shifts features up or down with respect to the non-refractive Rayleigh continuum (short-dashed line). In spectral region where molecular absorption is not much stronger than Rayleigh scattering, i.e. from 0.7 to 2 μm for H_2O , the size of absorption features are pretty sensitive to the abundance of the responsible

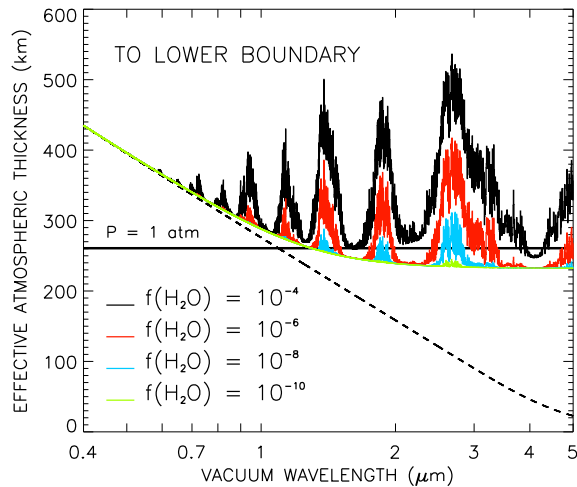


Figure 5. Transmission spectra with refraction of a Jupiter-sized exoplanet, with a 300 K isothermal Jovian atmosphere for various vertical homogeneous mole fractions of water (see inset legend), if one could somehow probe the atmosphere to the lower refractive boundary, irrespective of the planet-star distance. The non-refractive Rayleigh continuum (short-dashed curve) is shown for comparison.

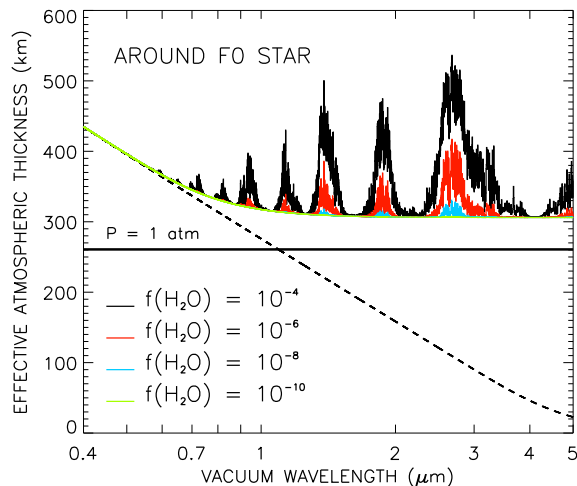


Figure 6. Transmission spectra with refraction of a Jupiter-sized exoplanet, with a 300 K isothermal Jovian atmosphere for various vertical homogeneous mole fractions of water (see inset legend), orbiting a F0 star. The non-refractive Rayleigh continuum (short-dashed curve) is shown for comparison.

species. However, with the rapid decrease with wavelength of the Rayleigh scattering cross section, water abundances can change by several orders of magnitude above a certain threshold with hardly a change in the size of the spectral features in the infrared. In this regime, small changes in the retrieved planetary radius can compensate for several orders of magnitude of change in the retrieved abundance (Griffith 2014), thus resulting in certain retrieval degeneracies when faced with noisy data or data obtained only in the infrared.

Figure 4 also shows that much of the water features for

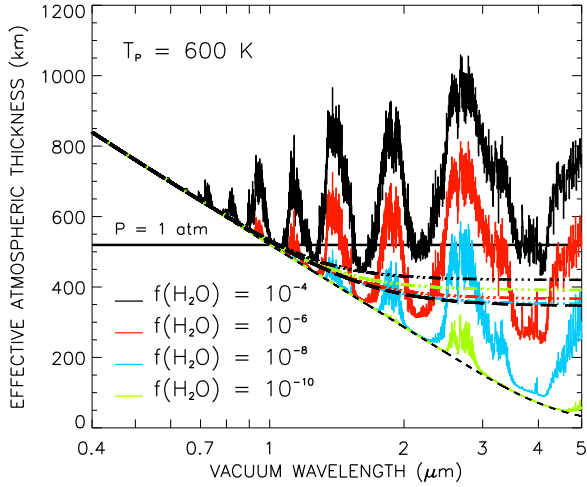


Figure 7. Transmission spectra without refraction of a Jupiter-sized exoplanet with a 600 K isothermal Jovian atmosphere for various vertical homogeneous mole fractions of water (see inset legend). The water-free Rayleigh scattering transmission spectra from Fig. 2 are overlaid for comparison (see caption and inset legend in Fig. 1 for more details). Refraction will suppress water features which lie below the refractive Rayleigh curve associated with the host star’s spectral type (coloured triple-dotted dashed lines).

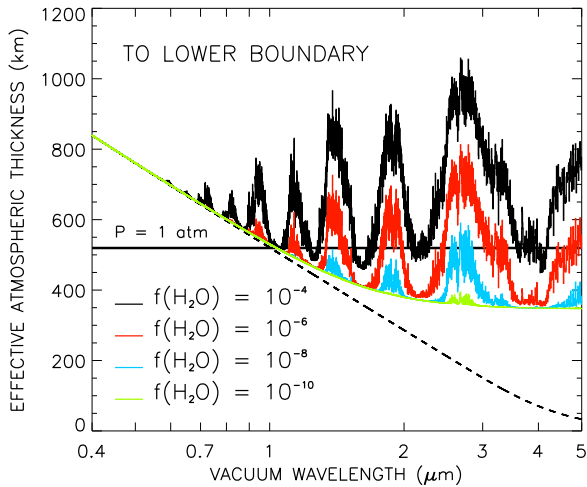


Figure 8. Transmission spectra with refraction of a Jupiter-sized exoplanet, with a 600 K isothermal Jovian atmosphere for various vertical homogeneous mole fractions of water (see inset legend), if one could somehow probe the atmosphere to the lower refractive boundary, irrespective of the planet-star distance. The non-refractive Rayleigh continuum (short-dashed curve) is shown for comparison.

the non-refractive case can lie below the refractive Rayleigh continuum, depending on the water abundance and the spectral type of the host star. As these features will be severely decreased in the refractive case, Figure 4 illustrates the fraction of water features that can be hidden by refraction for various scenarios. In the refractive case, the size of absorp-

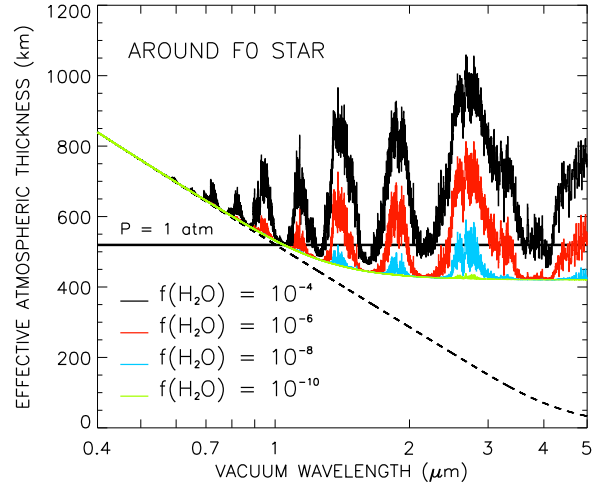


Figure 9. Transmission spectra with refraction of a Jupiter-sized exoplanet, with a 600 K isothermal Jovian atmosphere for various vertical homogeneous mole fractions of water (see inset legend), orbiting a F0 star. The non-refractive Rayleigh continuum (short-dashed curve) is shown for comparison.

tion features increases as the critical boundary decreases in altitude. The maximum size occurs if one can somehow probe down to the lower refractive boundary, which is shown in Figure 5. Since the effective scaleheight of the atmosphere tends to zero toward the lower refractive boundary, refraction reduces the size of spectral features the closer they are to this boundary. This is particularly obvious with the peak of the water feature at $2.7 \mu\text{m}$ for various abundances. Without refraction (Figure 4), the size of this feature for a mole fraction of 10^{-10} (green solid line), is similar to the part of the feature above the long-dashed solid line for a mole fraction of 10^{-8} (blue solid line). However, their sizes in the refractive case (Figure 5) are completely different.

What is particularly interesting about Figure 5 is that, unlike in the non-refractive case, the size of spectral features in the infrared varies dramatically with the abundance of the absorbing species. Hence, the retrieval degeneracy described by Griffith (2014) does not exist for a cloud-free 300 K cool atmosphere because the refractive lower boundary provides a reference altitude akin to a surface below which spectral features cannot exist. Furthermore, the boundary which is relevant for the retrieval of atmospheric properties is the critical boundary, which raises the refractive continuum and decreases the size of spectral features further, and more so for hotter stars than for cooler stars. Amongst the spectral type that I have considered (see Table 2), a planet orbiting an F0 star has the smallest spectral features. Figure 6 shows that around a F0 star a 300 K atmosphere with a water mole fraction of 10^{-10} does not have any recognisable features, and an abundance of 10^{-8} produces only weak features, contrary to what is observed for the non-refractive case (Figure 4).

The breaking of this degeneracy is not due to opacity from Rayleigh scattering but rather by two refractive effects also responsible for the decrease of the Rayleigh slope:

- The decrease of the effective scaleheight of the atmo-

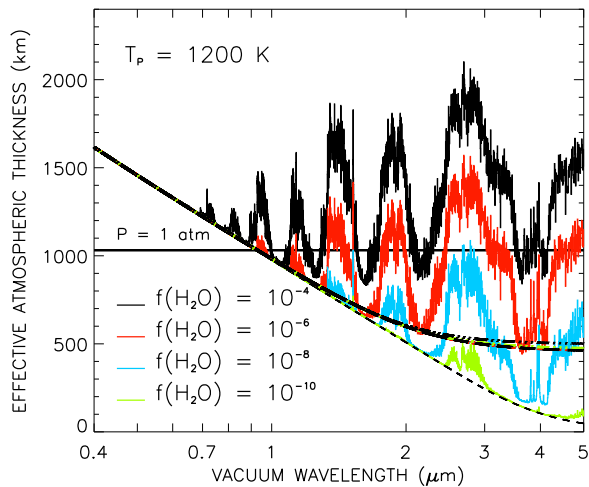


Figure 10. Transmission spectra without refraction of a Jupiter-sized exoplanet with a 1200 K isothermal jovian atmosphere for various vertical homogeneous mole fractions of water (see inset legend). The water-free Rayleigh scattering transmission spectra from Fig. 3 are overlaid for comparison (see caption and inset legend in Fig. 1 for more details). Refraction will suppress water features which lie below the refractive Rayleigh curve associated with the host star’s spectral type (coloured triple-dotted dashed lines).

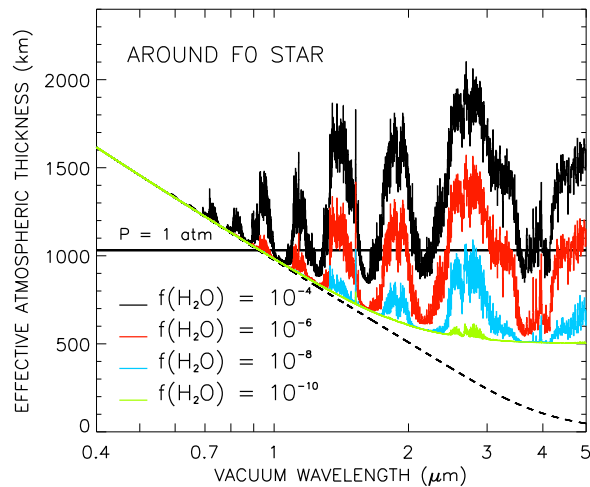


Figure 12. Transmission spectra with refraction of a Jupiter-sized exoplanet, with a 1200 K isothermal jovian atmosphere for various vertical homogeneous mole fractions of water (see inset legend), orbiting a F0 star. The non-refractive Rayleigh continuum (short-dashed curve) is shown for comparison.

the atmosphere, just as a surface or an optically thick cloud does.

These two effects create a refractive continuum which manifests itself in the infrared, where Rayleigh scattering is weak, in spectral regions of low molecular opacity.

Figures 7–9, and Figures 10–12 display the same information as Figures 4–6, but for planetary temperatures of 600 and 1200 K, respectively. Aside from the scaling of the size of the spectral features with temperature, one can observe only subtle changes with temperature in the overall shape of the spectral features in the non-refractive case (see Figures 4, 7, and 10). In the refractive case, as the planetary temperature increases, differences in the spectral type of the host star becomes less important and are almost negligible at 1200 K (compare Figures 11 and 12). Also, the size of spectral features varies with abundances but these variations are not as pronounced for the hotter exoplanets as the cooler exoplanets (e.g. compare Figures 5, 8, and 11 when one can probe to the lower boundary). This occurs because, as the planetary temperature increases, the refractive continuum is lower relative to the non-refractive H₂O spectral features, and thus has a correspondingly lower impact on the shape of these features.

At temperatures of 1200 K, a water mole fraction of 10⁻⁶ or higher produces spectral features which are largely unaffected by refraction, a result that seems consistent with Hubbard et al. (2001). However, including refraction allows one to constrain the possible range of abundances better. If one observes strong features in the data then small abundances are excluded. Conversely, the non-detection of spectral features need no longer be explained only with clouds, but can also with low abundances.

What happens to inferred abundances if an optically thick cloud deck is located at a lower density or pressure, or higher altitude, than the critical boundary? In this case, the cloud deck will raise the continuum and cut down the

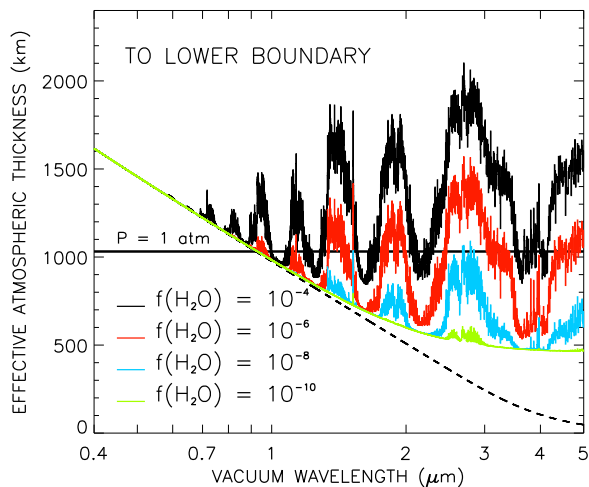


Figure 11. Transmission spectra with refraction of a Jupiter-sized exoplanet, with a 1200 K isothermal jovian atmosphere for various vertical homogeneous mole fractions of water (see inset legend), if one could somehow probe the atmosphere to the lower refractive boundary, irrespective of the planet-star distance. The non-refractive Rayleigh continuum (short-dashed curve) is shown for comparison.

sphere toward a value of zero as rays approach the lower boundary.

- The deflection, away from the observer, of rays grazing atmospheric regions below the critical altitude. This creates a step function with altitude in the perceived illumination of

size of spectral features even further than refraction does, so that the spectral features might have the same size as if produced by a lower abundance in a clear atmosphere. Hence, if one assumes that the atmosphere is cloud-free, abundances inferred from transmission spectra will be lower limits.

4 CONCLUSIONS

I investigated the effects of refraction on transmission spectra of giant exoplanets with a suite of simple isothermal atmospheric models for a Jupiter-like exoplanet with a Jovian H₂-He composition, ignoring stellar limb-darkening. The effects are particularly important for giant exoplanets, more so than for terrestrial exoplanets, because they do not possess a surface which could otherwise limit the density, or pressure, to which one can probe their atmosphere.

Indeed, without refraction, one can probe a pure Jovian H₂-He Rayleigh scattering atmosphere to more than 500 bar of pressure at 5 μm , barring other sources of extinction. However, refraction creates a thin refractive boundary layer at high densities where the perceived density scaleheight of the atmosphere is dramatically smaller than the actual scaleheight (B  tr  mieux & Kaltenegger 2015). This apparent decrease in the scaleheight reduces the size of spectral features and decreases the Rayleigh scattering slope within that layer.

The lower boundary of this refractive boundary layer is defined where the refraction-induced curvature of a ray allows it to follow a circular trajectory around the planet. Atmospheric regions below this boundary can never be probed during an exoplanetary transit. This flattens out the Rayleigh continuum in the infrared and effectively mimics a surface. The pressure level of this lower refractive boundary increases with temperature and is much lower than in the non-refractive case. It varies from a pressure of 5.4 to 86.3 bar as the atmospheric temperature changes from 300 to 1200 K in an isothermal Jovian atmosphere.

The flat infrared Rayleigh continuum that one obtains with refraction is significantly different from the non-refractive case, where the Rayleigh continuum decreases with wavelength with a slope characteristic of the scaleheight of the atmosphere. At shorter wavelengths, the refractive Rayleigh continuum slowly merges with the non-refractive one. The wavelength above which refraction changes significantly the Rayleigh slope increases with temperature, from about 0.6 to 1 μm between atmospheric temperatures of 300 and 1200 K. Accounting for the angular size of the host star seen from the planet, raises the Rayleigh continuum and changes the Rayleigh slope further, which shifts this spectral boundary to lower wavelengths.

The magnitude of this correction can be quite substantial for an atmospheric temperature of 300 K and for a F0 spectral type host star, but decreases with decreasing stellar temperature and with increasing atmospheric temperature. At atmospheric temperatures of 1200 K, the correction for a planet around an F0 star is very small. At this temperature, the transmission spectrum is almost independent of the spectral type of the host star and is mostly determined by the location of the lower refractive boundary.

As I illustrated with water absorption features, the re-

duced effective scaleheight near the lower boundary and the step function in the apparent illumination of the atmosphere at the critical boundary, also responsible for the reduction of the Rayleigh slope, break the retrieval degeneracy between abundances and planetary radius. In the non-refractive case, when absorption is much stronger than Rayleigh scattering, changes of several orders of magnitude in the mole fraction of well-mixed species only shifts the spectrum up or down in effective radius without changing the size of spectral features significantly. However, in the refractive case, the size of H₂O features changes dramatically with abundances for a 300 K atmosphere. As the atmospheric temperature increases, the refractive continuum shifts downward relative to spectral features, and the variation with abundance of the size of spectral features decreases. At atmospheric temperatures of 1200 K, only water mole fraction lower than 10^{-6} show some significant size variation with abundance.

The possible presence of an optically thick cloud deck complicates retrieval of atmospheric properties further. The abundances obtained from assuming a clear atmosphere are lower limits. However, the brighter refractive wings just outside of transit can be used to distinguish between clear and cloudy atmospheres (Misra & Meadows 2014). Hence, it is clear that including all effects of refraction in exoplanet atmosphere retrieval algorithms can only help constrain atmospheric properties.

Although quite important even for hot exoplanets, refractive effects are more pronounced in cooler atmospheres. Even though the bulk of exoplanet observations has been primarily focused on hot exoplanets because they are easier to detect and characterise, long-time monitoring of various areas of the sky is just starting to yield longer-period cooler exoplanets (Crossfield et al. 2015, Jenkins et al. 2015) with promises of more to come. Furthermore, with the upcoming planned launches of the Transiting Exoplanet Survey Satellite (TESS) and the James Webb Space Telescope (JWST), it is only a matter of time before we start obtaining exoplanet transmission spectra of sufficient quality that signatures of refraction can be exploited to constrain the atmospheric properties of planets of any temperature.

ACKNOWLEDGEMENTS

I wish to thank the directors of the Max-Planck-Institut f  r Astronomie, Thomas Henning and Hans-Walter Rix, who have graciously provided a fantastic research environment and facilities for one full year above and beyond the end of my contract. This research, as well as that in B  tr  mieux & Kaltenegger (2015), would not have been possible otherwise.

REFERENCES

- Baum W. A., Code A. D., 1953, *AJ*, 58, 108
- Benneke B., Seager S., 2012, *ApJ*, 753, 100
- B  tr  mieux Y., Kaltenegger L., 2013, *ApJ*, 772, L31
- B  tr  mieux Y., Kaltenegger L., 2014, *ApJ*, 791, 7
- B  tr  mieux Y., Kaltenegger L., 2015, *MNRAS*, 451, 1268
- Brown T. M., 2001, *ApJ*, 553, 1006

- Cox A. N., 2000, *Allen's Astrophysical Quantities*, 4th edn., AIP, New York
- Crossfield I. J. M., Petigura E., Schlieder J. E., Howard A. W. et al., 2015, *ApJ*, 804, 10
- de Wit J., Seager S., 2013, *Science*, 342, 1473
- Ford A. L., Browne J. C., 1973, *Atomic data*, 5, 305
- García Muñoz A., Zapatero Osorio M. R., Barrena R., Montañés-Rodríguez P., Martín E. L., Pallé E., 2012, *ApJ*, 755, 103
- Griffith C. A., 2014, *Phil. Trans. R. Soc. A*, 372, 20130086
- Howe A. R., Burrows A. S., 2012, *ApJ*, 756, 176
- Hubbard W. B., Fortney J. J., Lunine J. I., Burrows A., Sudarsky D., Pinto P., 2001, *ApJ*, 560, 413
- Hui L., Seager S., 2002, *ApJ*, 572, 540
- Jenkins J. M., Twicken J. D., Batalha N. M., Caldwell D. A. et al., 2015, *AJ*, 150, 56
- Johnson D. G., Jucks K. W., Traub W. A., Chance K. V., 1995, *JGR*, 100, 3091
- Jordán A., Espinoza N., Rabus M., Eyheramendy S., Sing D. K. et al., 2013, *ApJ*, 778, 184
- Kaltenegger L., Traub W. A., 2009, *ApJ*, 698, 519
- Knutson H., Charbonneau D., Noyes R. W., Brown T. M., Gilliland R. L., 2007, *ApJ*, 655, 564
- Lecavelier des Etangs A., Pont F., Vidal-Madjar A., Sing D., 2008, *A&A*, 481, L83
- Lodders K., Fegley Jr. B., 1998, *The Planetary Scientist's Companion*, Oxford Univ. Press, New York
- Mancini L., Southworth J., Ciceri S. et al., 2014, *MNRAS*, 443, 2391
- Mansfield C. R., Peck E. R., 1969, *J. Opt. Soc. Am.*, 59, 199
- Misra A. K., Meadows V. S., 2014, *ApJ*, 795, L14
- Misra A., Meadows V., Crisp D., 2014, *ApJ*, 792, 61
- Nascimbeni V., Piotto G., Pagano I. et al., 2013, *A&A*, 559, A32
- Nikolov N., Sing D. K., Burrows A. S., Fortney J. J., Henry G. W. et al., 2015, *MNRAS*, 447, 463
- Pont F., Knutson H., Gilliland R. L., Moutou C., Charbonneau D., 2008, *MNRAS*, 385, 1, 109
- Reid I. N., & Hawley, S. L. 2005, *New Light on Dark Stars: Red Dwarfs, Low-Mass Stars, Brown Dwarfs*, ed. I. N. Reid & S. L. Hawley, Springer-Praxis, New York, 169
- Robinson T. D., Maltagliati L., Marley M. S., Fortney J. J., 2014, *PNAS*, 111, 9042
- Sidis O., Sari R., 2010, *ApJ*, 720, 904
- Sing D. K., Vidal-Madjar A., Lecavelier des Etangs A., Désert J.-M., Ballester G., Ehrenreich D., 2008, *ApJ*, 686, 667
- Sing D. K., Lecavelier des Etangs A., Fortney J. J., Burrows A. S., Pont F. et al., 2013, *MNRAS*, 436, 2956
- Sing D. K., Wakeford H. R., Showman A. P., Nikolov N., Fortney J. J. et al., 2015, *MNRAS*, 446, 2428
- Smith G. R., Hunten D. M., 1990, *Rev. Geophys.*, 28, 117
- Southworth J., Mancini L., Maxted P. F. L. et al., 2012, *MNRAS*, 422, 3099
- Southworth J., Mancini L., Ciceri S. et al., 2015, *MNRAS*, 447, 711
- Swain M. R., Line M. R., Deroo P., 2014, *ApJ*, 784, 133
- Traub W. A., Stier M. T., 1976, *ApOpt*, 15, 364
- Wakeford H. R., Sing D. K., 2015, *A&A*, 573, A122
- Weber M. J., 2003, *Handbook of optical materials*, CRC Press LLC, Boca Raton, FL